

# Non-Affine Shear Modulus in Entangled Networks of Semiflexible Polymers

Hauke Hinsch<sup>1</sup> and Erwin Frey<sup>1</sup>

Arnold Sommerfeld Center for Theoretical Physics and Center of NanoScience,  
Department of Physics, Ludwig-Maximilians-Universität München,  
Theresienstrasse 37, D-80333 München, Germany,

Received: date / Revised version: date

**Abstract.** We investigate the viscoelastic properties of entangled networks of semiflexible polymers. At intermediate time scales the elastic response of these networks to shear deformation is described by the plateau modulus  $G$ . Different scaling laws with polymer concentration  $c$  have been proposed based on the assumption that the deformation field is affine on all length scales. We develop a numerical approach that allows to calculate the modulus via free energy changes for both affine and non-affine deformations. The non-affine deformation field is obtained by a free energy minimization. Our findings allow for a confirmation of a power law  $G \propto c^{7/5} l_p^{-1/5}$  with polymer concentration  $c$  and persistence length  $l_p$  and furthermore quantify the systematic deviations due to the affinity assumption.

**PACS.** 87.16.Ka Filaments, microtubules, their networks, and supramolecular assemblies – 87.19.rd Elastic Properties – 62.25.-g Mechanical properties of nanoscale systems

## 1 Introduction

Semiflexible polymers have always been an interesting testing ground for concepts of statistical physics, since excitable energies are on the order of  $k_B T$ , fluctuations are important and entropic effects compete with bending energy. However, with a few exception like the tangent-tangent correlation function [1, 2], moments of the end-to-end distance [3] in the wormlike-chain model [4, 3] or the end-to-end distribution function [5] in the weakly-bending rod approximation, a multitude of interesting single polymer properties are not accessible to analytic solutions. This applies even more so to many-polymer systems like networks or solutions. In these cases, inter-polymer interactions or topological constraints complicate the theoretical treatment and the mere number of constituents and degrees of freedom clearly renders any analytical attempt to calculate the partition sum unfeasible. Our line of approach is therefore to reduce the many-body problem to a single-polymer description. A prominent example of such an approach is the tube model introduced by de Gennes [6] and Doi and Edwards [1] that describes the combined effect of neighboring polymers by a mean-field potential. These theoretical models for single polymers at hand, one can proceed to describe macroscopic properties of a polymeric material. Here it is essential to build on the microscopic constituents without losing emerging collective properties of the macroscopic material.

These material properties of polymer networks are of a stunning variety and complexity. Spurred by the biological importance of networks of filamentous actin (F-actin), intensive experimental research has recently focussed on this model system. In the presence of cross-links polymer solution form permanent gels or bundles with different elastic properties determined by a competition of bending and stretching modes [7, 8, 9, 10]. Recently, also the importance of non-affine deformations has been pointed out [11]. For purely entangled solutions a strong dependence of both the storage and the loss modulus on frequency was observed [12, 13, 14, 15]. Furthermore, similarities to glassy systems were reported [16, 17]. Upon application of larger stress a non-linear regime was investigated and shear stiffening of the network was observed [18, 19]. Theoretical analysis identified different scaling regimes for the moduli with frequency [20]. Regarding the scaling of the plateau modulus with concentration Isambert and Maggs derived a power-law of 7/5 from a simple scaling argument [21] based on the deformation of confinement tubes. Other theories attribute the material response to the suppression of undulations by stretching [7, 22]. They predict a scaling with a considerably larger exponent, but seem to disagree with experimental data [23, 24, 25]. Recent experimental work [26] claims to have verified an exponent of 4/3 predicted by an elastic medium theory [14]. Common to all these approaches is the assumption that the macroscopic deformation field is assumed to be affinely transmitted to all length scales. We will present an ap-

proach that permits to go beyond this assumption and investigate resulting differences.

We proceed as follows: in Section 2 we define the system under consideration. We introduce the Hamiltonian of the network, review the simplifications that lead to the tube model and prior work on the plateau modulus, and emphasize the mean-field nature of the tube model and the assumption of affine displacement. In Section 3 we present our approach to numerically compute the free energy of the system by a reduction to two dimensions. We explain the effect of global shear on the microscopic constituents of the network and introduce a free energy minimization procedure that results in a non-affine deformation field. We proceed in Section 4 with the presentation and interpretation of our results before we conclude in Section 5.

## 2 System Definition

We consider a network of semiflexible polymers that only interact via a hard-core potential and thus constrain each other topologically. The polymer density is given by the number  $\nu$  of polymers of length  $L$  per unit volume. The stiffness  $\kappa$  of the polymers gives rise to a persistence length of  $l_p = \kappa/k_B T$ . The configuration of the  $i$ -th polymer in space,  $\mathbf{r}_i(s)$ , is parameterized by arc length  $s$  and the average distance between the networks constituents is characterized by the mesh size,  $\xi = \sqrt{3/\nu L}$ . Concerning the mechanical response of the network, we are interested in the dynamic processes that occur after a deformation has driven the system out of equilibrium. These relaxation processes occur on different time scales. While generally every stress can relax by reptation of the polymers, this process is dramatically slowed down due to topological constraints in crowded environments [27,28]. On intermediate time scales relevant for the plateau modulus it can be assumed that the constraints imposed by surrounding polymers can not be overcome and that the center of mass of all filaments does not change substantially. A given polymer  $i$  is then described by the worm-like chain model [4,3] with a Hamiltonian that has contributions from intra-polymer bending and from interactions with the neighboring filaments in the solution. This can be written as

$$H_i = \frac{\kappa}{2} \int_0^L ds \left( \frac{\partial^2 \mathbf{r}_i(s)}{\partial s^2} \right)^2 + \sum_{j \neq i} \Theta_{i,j}^{\mathcal{I}}, \quad (1)$$

where the function  $\Theta_{i,j}^{\mathcal{I}}$  formally describes the hard-core interaction between the polymers  $i$  and  $j$  under the initial topology  $\mathcal{I}$ . Note that this function does not only depend on the configurations  $\mathbf{r}_i(s)$  and  $\mathbf{r}_j(s)$  of the polymers like a conventional hard-core potential that would always be zero in a system of mathematical lines without excluded volume. Instead it crucially depends on the initial topology and rules out polymer crossing by returning an infinite energy if the two polymers interpenetrate <sup>1</sup>. The Hamiltonian of the complete system is obtained as  $H = \sum_i H_i$ .

<sup>1</sup> For times far larger than the relevant time scale for the plateau modulus the contributions  $\Theta_{i,j}^{\mathcal{I}}$  vanish as topological

Given the form of the Hamiltonian (1) a calculation of the free energy  $F$  from the partition sum  $Z$  as  $F = -k_B T \ln Z$  is obviously not feasible as the partition sum

$$Z = \Pi_i \int \mathcal{D}[\mathbf{r}_i(s)] \exp[-H/(k_B T)] \quad (2)$$

amounts to multiple path integrals of a highly convoluted integrand.

A simplifying description of the system was proposed with the famous tube model [6,1] where the combined effect of the fluctuating neighbor polymers on a single test polymer is described by an effective harmonic potential. While the tube model is the foundation for theories for different properties of semiflexible polymer networks like tube diameter [29,14,30] or viscoelasticity [21], it has to be kept in mind that it only provides a mean-field description of the microscopic constituents. In the remainder of this section we will review how free energies and mechanical properties can be derived from the tube model and point out possible shortcomings of this coarse-grained frame of description.

The tube model can be applied to solutions of semiflexible polymers where the confinement of a single polymer by its neighbors is sufficiently strong to guarantee that the transversal undulations of the polymer do not deviate far from an average contour in space - the tube backbone  $\mathbf{r}^0(s)$ . This is the case, if persistence length and polymer contour length are substantially larger than the typical void spaces in the mesh of surrounding polymers, thus  $L, l_p \gg \xi$  as e.g. given for most F-actin networks. The complex sum in the second term of the Hamiltonian (1) can then conveniently be substituted by a harmonic potential with average strength  $\gamma$  and minimum at the tube backbone:

$$H(\gamma, \kappa) = \int_0^L ds \left[ \frac{\kappa}{2} \left( \frac{\partial^2 \mathbf{r}(s)}{\partial s^2} \right)^2 + \frac{\gamma}{2} (\mathbf{r}(s) - \mathbf{r}_0(s))^2 \right]. \quad (3)$$

As pointed out by Odijk [31] it is instructive to introduce an additional length scale  $L_d \approx (\nu L)^{-2/5} l_p^{1/5}$  known as deflection or Odijk length. While the length scales  $L$  and  $l_p$  describe the properties of the single polymer and the length scale  $\xi$  describes the network, the deflection length  $L_d$  captures the interaction between both. It can be interpreted as a measure for the distance between two collisions between the encaged polymer and the tube walls and therefore the number of collisions of a polymer is given as  $L/L_d$ . This is also reflected in the free energy cost  $\Delta F$  that arises from the restriction of the test polymer to a tube and is obtained by a path integration of (3) over all polymer configurations [32] as

$$\Delta F = \sqrt{2} k_B T \frac{L}{L_d}. \quad (4)$$

constraints can be overcome by reptation. This signifies that long time averages will reproduce the results obtained from an ensemble average with respect to the free polymer Hamiltonian.

This signifies that at a spacing of  $L_d$  between two collisions every of the  $L/L_d$  contact points between polymer and tube contributes one  $k_B T$  to the confinement free energy.

Having derived the free energy in the coarse-grained tube model, the next step is to analyze the change in free energy at mechanical deformation to obtain the plateau modulus. As the polymers are described in terms of their tubes, it is obvious to investigate the effect of deformation on the tubes for which the free energy is known as reasoned above. Together with a scaling law  $d \propto c^{-3/5} l_p^{-1/5}$  for the tube diameter  $d$  derived by Semenov [29] this line of reasoning was first used by Isambert and Maggs [21] to establish a scaling relation between plateau modulus and concentration. They argue that the macroscopic shear deformation is affinely passed down to the tubes that are compressed or stretched depending on their orientation to the shear. The resulting change of the tube diameter causes a change in the deflection length  $L_d$  and with the help of (4) the resulting modulus scales as

$$G \propto c^{7/5} l_p^{-1/5}. \quad (5)$$

The same scaling was also obtained by other descriptions, *e.g.* by a modified Onsager theory for confinement tubes [23]. In an endeavour to arrive at a quantitative theory for the plateau modulus Morse [14] has proposed two conceptually different approaches: a detailed microscopic description of the topological constraint imposed by neighboring polymers leads him to the prediction of a modulus scaling with  $c^{7/5}$  and a quite different approach yields a scaling of  $G \propto c^{4/3}$  derived by a self-consistent treatment of the network as an elastic continuum. Since these values are numerically quite close, a decisive distinction between the models has not yet been possible with the accuracy of available experimental data.

It has to be kept in mind that all these theoretical approaches are implicitly build on the assumption that the tube contour deforms affinely with the macroscopic strain. This is evidently only a very coarse-grained description of the system's response. While stress relaxation by slow processes like reptation is obviously not relevant on the time scale of the plateau modulus, it is however possible that faster relaxation processes cause a tube contour that differs from the contour obtained by affine displacement. Our goal is to implement this relaxation processes by a free energy minimization in a numerical solution of the plateau modulus and investigate the quantitative and qualitative differences to the affine model. The detailed setup of this approach is discussed in the following section.

### 3 Numerical Solution

Our approach is to obtain a numerical solution of the partition sum (2) for a test polymer in a typical network of semiflexible polymers by averaging over all allowed configurations of neighboring polymers. The advantage of this approach is a microscopic description of the Hamiltonian. In contrast to the tube-model that only provides a coarse-grained description of the surrounding polymers, it accounts for the detailed interactions in a given realization

of disorder. This permits to investigate the effect of local non-affine deformations of the encaged test polymer. Since the distribution of obstacle polymers around a given test filament is quite heterogeneous, it is expected that these non-affine deformations result in a lower global free energy. Our aim is to find this free energy minimum by a numeric minimization procedure.

#### 3.1 Reduction to 2D

To reach this goal, we start by decomposing the transverse undulations of the test polymer into two independent components as previously described [33]. For one component the Hamiltonian thus simplifies to the description of a two-dimensional polymer in a plane surrounded by a certain number  $N_{\text{obs}}$  fluctuating point-like obstacles (see Fig. 1). The point-like obstacles are subjected to a harmonic

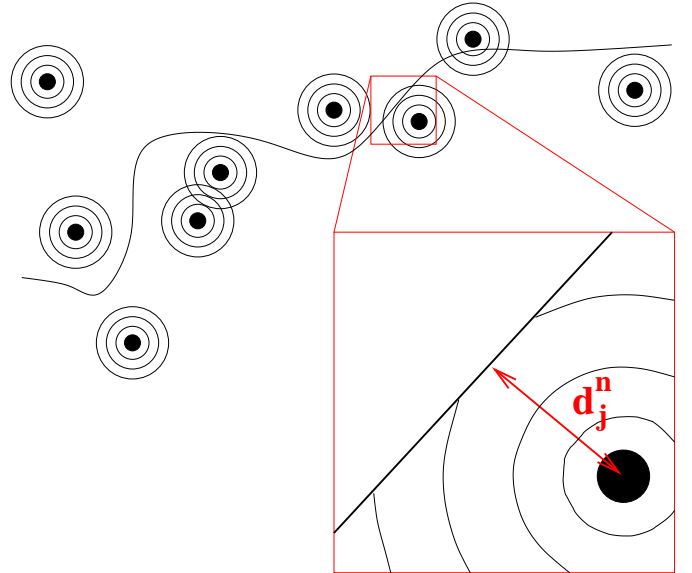


**Fig. 1.** Fixed polymer in an array of fluctuating point obstacles (black points). The interaction between the polymer and the obstacles as the fluctuations of the  $j$ -th point obstacle are hindered by the polymer at a distance  $d_j^n$  (see inset).

potential with strength  $\gamma$  around an equilibrium position  $\mathbf{p}_j^0$  with  $j = 1, \dots, N_{\text{obs}}$ . The parameters  $N_{\text{obs}}$  and  $\gamma$  can be chosen to self-consistently represent a network of a specific concentration [30]. Therefore the system is completely described by the two-dimensional contour  $\mathbf{r}(s)$  of the test polymer and  $N_{\text{obs}}$  two-dimensional vectors  $\mathbf{p}_j$  describing the positions of the obstacles in the plane. The Hamiltonian thus reads  $H = H^p + \sum_{j=1}^{N_{\text{obs}}} H_j^{\text{obs}}$  where  $H^p$  is the bending energy contribution from the polymer

$$H^p = \frac{\kappa}{2} \int_0^L ds \left( \frac{\partial^2 \mathbf{r}(s)}{\partial s^2} \right)^2 \quad (6)$$

and the  $H_j^{\text{obs}}$  are the contributions from the obstacle points

$$H_j^{\text{obs}} = \frac{\gamma}{2} (\mathbf{p}_j - \mathbf{p}_j^0)^2 + \Theta[\mathbf{r}(s), \mathbf{p}_j, \mathbf{p}_j^0], \quad (7)$$

where the topological constraint of uncrossability is again described by a function  $\Theta$  that returns an infinite energy if the polymer and a point obstacle cross. In contrast to the three-dimensional case Eq. (1) this function can now easily be grasped geometrically as we will show below. In calculating the corresponding partition sum we have to solve

$$Z = \int \mathcal{D}[\mathbf{r}(s)] \int \prod_{j=1}^{N_{\text{obs}}} d\mathbf{p}_j \exp[-\beta H^p] \exp[-\beta \sum_{j=1}^{N_{\text{obs}}} H_j^{\text{obs}}]. \quad (8)$$

While the description has now reduced to a single path integral, an analytical solution is still complicated by the topological constraints. However, for a specific polymer contour, the integration over the degrees of freedom of the obstacles is straightforward and can easily be carried out analytically as the only topological restriction for each point obstacle is posed by the test polymer. Since the polymer is mostly straight on the length scale of the typical fluctuation width of an obstacle, we assume that integration over the obstacle potential is performed only in the half-space that is limited by the test polymer at a nearest normal distance  $d_j^n$  as depicted in Fig. 1. The partition sum is then written as:

$$Z = \int \mathcal{D}[\mathbf{r}(s)] \exp[-\beta H^p] \prod_{j=1}^{N_{\text{obs}}} \frac{\pi}{\gamma} \text{erfc} \left[ -d_j^n \sqrt{\frac{\gamma}{2}} \right]. \quad (9)$$

To solve the remaining path integration we chose to apply a saddle point approximation in which we first assume the test polymer to be immobile. Then we find the fixed contour that maximizes the partition sum and thereby minimizes the free energy and finally add fluctuations around this minimum. In the first step we are faced with the minimization problem depicted in Fig. 1. An immobile polymer with associated bending stiffness is placed in an array of fluctuating obstacles. The free energy is composed of the bending energy of the polymer and the entropic contributions from the obstacles. It is obtained from the partition sum from Eq. (9) and is a function of the polymer contour  $\mathbf{r}(s)$  alone:

$$F(\mathbf{r}(s)) = H^p(\mathbf{r}(s)) + \sum_{j=1}^{N_{\text{obs}}} -k_B T \ln \left( \frac{\pi}{\gamma} \text{erfc} \left[ -d_j^n \sqrt{\frac{\gamma}{2}} \right] \right). \quad (10)$$

We are now looking for the contour  $\mathbf{r}^0(s)$  of the polymer that minimizes the free energy for a given initial setup of obstacles.

### 3.2 Free Energy Minimization

Technically, this contour is obtained as follows. We start from a given initial polymer configuration and choose  $N_{\text{min}}$  nodes as a discretization along its contour. This reduces the required minimization to  $N_{\text{min}}$  dimensions and permits to obtain a feasible computation time by a suitable choice of  $N_{\text{min}}$ . To find the minimum of the free energy,

Eq.(10), we move these nodes certain distances transverse to the present polymer contour, and define the new trial contour as a cubic spline through the new node positions; here one has to make sure that total contour length is kept constant. With this new contour both the bending energy and the entropic contribution to the free energy is computed according to Eq.(10). These steps of moves transverse to the immediately preceding contour are repeated until the minimum of the free energy is reached. The minimization algorithm we used is based on the AMOEBA [34] implementation of the Neelder-Mead method [35].

### 3.3 Mode Representation

Now that we have found the polymer contour of lowest free energy, we proceed to add the transversal fluctuations of the polymer in form bending modes. The contour of min-

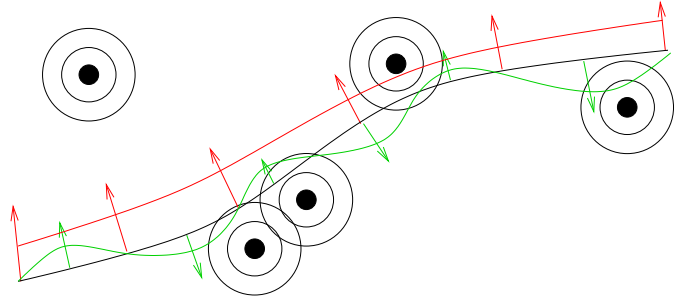


**Fig. 2.** Modes  $k = 0$  (red) and  $k = 3$  (green) around the contour of minimal free energy (black).

imal free energy  $\mathbf{r}^0(s)$  can be interpreted as the backbone of the test polymer's confinement tube or the contour with the highest probability. All deviations from this contour have higher free energy and thus a smaller probability. We model the thermal undulations of the polymer around this tube backbone by cosine modes  $u_k(s)$  in the form

$$r_{\perp}(s) = \sum_k u_k(s) = \sum_k A_k \cos\left(\frac{sk}{L}\right) \quad (11)$$

where  $k$  is the mode number and  $A_k$  is the mode amplitude. In this representation the mode  $k = 0$  is simply a transversal displacement of every point of the polymer normally to  $\mathbf{r}^0$ . A visualization of this mode and the mode  $u_{k=3}$  is depicted in Fig. 2. For a specific mode we can monitor the resulting free energy as a function of the mode amplitude  $A_k$  as exemplary shown in Fig. 3. The result is a harmonic function  $F(A_k) = \omega_k/2A_k^2$  where  $\omega_k$  can be determined from the plots for every mode. The Hamiltonian for a certain contour that is in the representation (11) fully characterized by the set of coefficients  $\{A_k\}$  is then given as

$$H(\{A_k\}) = \frac{1}{2} \sum_k \omega_k A_k^2 \quad (12)$$

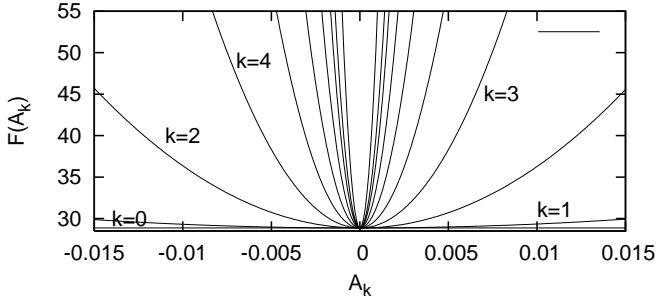


**Fig. 3.** Increase of free energy with amplitude for different modes in a given random array of obstacles.

The desired partition function can thus easily be obtained by integration over the mode amplitudes

$$Z = \prod_k dA_k \exp[-\beta\omega_k A_k^2/2] = \prod_k \sqrt{\frac{2\pi}{\beta\omega_k}}. \quad (13)$$

The free energy cost of confinement is obtained by calculating for every mode the free energy difference between a confined and a free polymer. Since  $\omega_k \propto k^4$  (compare Fig. 3) this difference becomes small quickly with increasing mode number  $k$  such that it suffices to compute the free energy difference for the first few modes.

### 3.4 Shear Deformation

Having developed an approach to calculate the free energy of a fluctuating polymer in an array of fluctuating topological constraints, we can proceed to investigate the free energy change as a reaction to shear deformations. A simple example of such a deformation is a global shear deformation of a macroscopic sample. If the sample is an equilibrated network of semiflexible polymers, the result of the shear deformation will be a rise in free energy and consequently a force counter-acting the deformation. The system is thus perturbed by the deformation and brought to a non-equilibrium state which will immediately be followed by relaxation processes. These relaxation processes occur on very different time scales for the different length scales in the network. This is the reason for the frequency dependence of the modulus.

For very long time for instance, the network is able to completely relax the deformation stress by reptation thereby recovering the equilibrium value of free energy and resulting in a vanishing modulus. We can assume that at the time scale of the plateau modulus the encaged polymers have completely experienced their immediate surroundings but no large scale relaxation by network rearrangement has occurred. Thus in measuring the plateau modulus the tube has sufficient time to form before the deformation field changes again. This argument is the foundation for the assumption of affine displacement of the tube's contour and size. As it is unknown how exactly the macroscopic stress is passed on to the microscopic constituents of the network, it is commonly assumed that

the deformation field follows the macroscopic stress on all length scales. Since at the time scale of the plateau modulus the tube is the relevant quantity, the tube centers or backbones are displaced affinely with the global shear. Translated to our two-dimensional plane of observation, this signifies that the tube contour  $\mathbf{r}^0(s)$  and the centers of the obstacle tube  $p_j^0$  are deformed affinely as depicted in Fig. 4 (top). The free energy of this new configuration can be calculated as shown above. The modulus  $G_A$  to be determined from this resulting free energy change should be equivalent to the modulus obtained from any theoretical treatment that is based on the assumption of affine displacement.

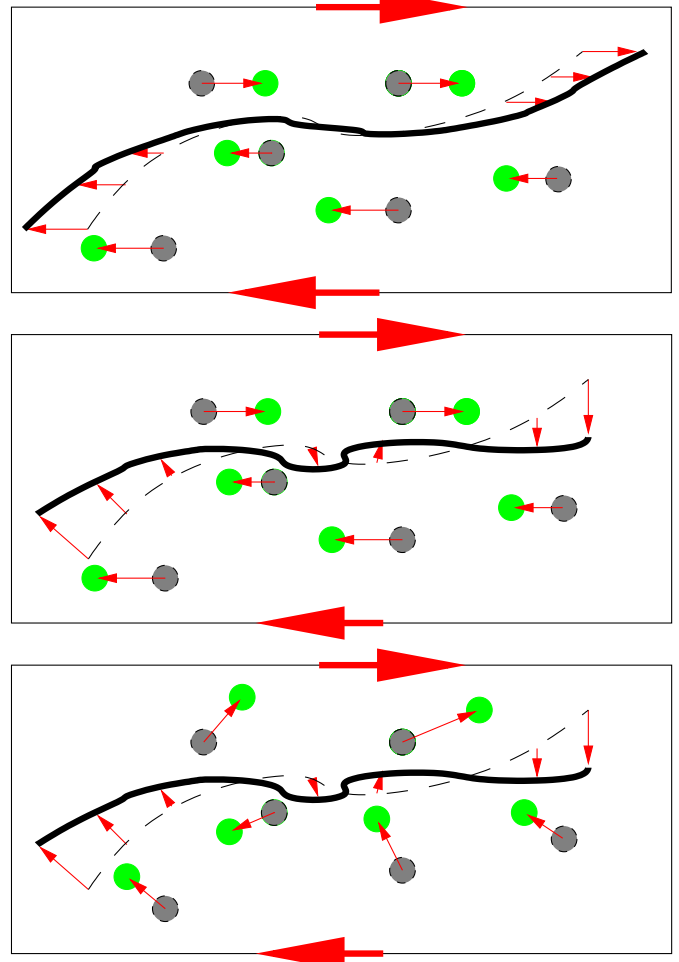


**Fig. 4.** Different levels of affinity in shear deformations. **(top)** Obstacle fluctuation centers and tube backbone follow the macroscopic shear deformation (large red arrow) affinely. **(middle)** While the obstacle fluctuation centers follow the macroscopic shear deformation affinely, the tube backbone can deviate from the affine deformation field in order to minimize the global free energy. **(bottom)** Also the obstacle point can react by non-affine deformation to the macroscopic shear.

If we take a closer look at the processes at tube formation, it becomes clear that the tube obtained by affine

deformation is not necessarily a valid description of the physical reality. To this end we relax the assumption of affine displacement in such a way, that we now only let the obstacle fluctuation center  $p_j^0$  deform affinely as illustrated in Fig. 4 (*center*). If this new configuration of the obstacle array is taken for granted, we have to ask the question how the test polymer engaged by the obstacles reacts to this conformational change. Out of all possible deformations of the test polymer only the one with the lowest free energy will actually be realized. Obviously, this new tube contour will only in very few cases equal the tube contour obtained by affine displacement of the original contour. The resulting free energy of this deformation will thus be less or equal to the free energy obtained by affine deformation and we can therefore also state that the resulting modulus  $G_{NA} \leq G_A$ . Technically, the free energy difference of this non-affine deformation of the tube contour is obtained by displacing the  $p_j^0$  affinely with the macroscopic stress (see A) and then applying again the free energy minimization as explained above to find the new tube contour.

Of course, also the fact that we deform the obstacle points affinely implies an assumption. In the actual physical system the obstacle points and with it the tube centers of the neighboring polymers are free to change their position in order to reach a global state of lower free energy (see Fig. 4 (*bottom*)). As these neighboring polymers however couple to other polymers outside our plane of observation, the incorporation of this feature would be tantamount to a minimization in all degrees of freedom of the network. This is obviously out of range of a numerical solution. The resulting modulus of a complete free energy minimization is the modulus  $G$  that would be observed in experiments. The modulus determined by our approach constitutes an upper bound for the experimental values and thus  $G \leq G_{NA}$ .

## 4 Results

In the previous section we presented an approximative numerical solution to the problem of finding the free energy change under shear deformation of a single probe polymer. This is obviously a quantity that can not be observed experimentally, but it can serve as the basis for the calculation of the macroscopic plateau modulus. To obtain this observable we have to add up the contributions from all polymers in the network under consideration. One single specific polymer is described in terms of the two dimensional plane of observation whose orientation in space is described by a set of angles  $(\theta, \phi, \psi)$  as described in Appendix A. Consequently, we have to perform an average over these isotropically distributed angles and furthermore we have to average over the quenched disorder that is generated by the different configurations of point-like obstacles in the observation plane. With the shear parameter  $\Gamma$  this procedure finally returns an average free energy function  $\Delta F(\Gamma) = g\Gamma^2/2$  from which the macroscopic modulus is obtained as  $G = 2\nu g$ . The factor 2 stems from the fact that every polymer is described by two planes

of observation corresponding to the two components of transverse fluctuation.

For a single polymer in a plane and one specific realization of obstacle disorder the resulting free energy function is exemplary shown in Fig. 5 (*top*). Since the absolute

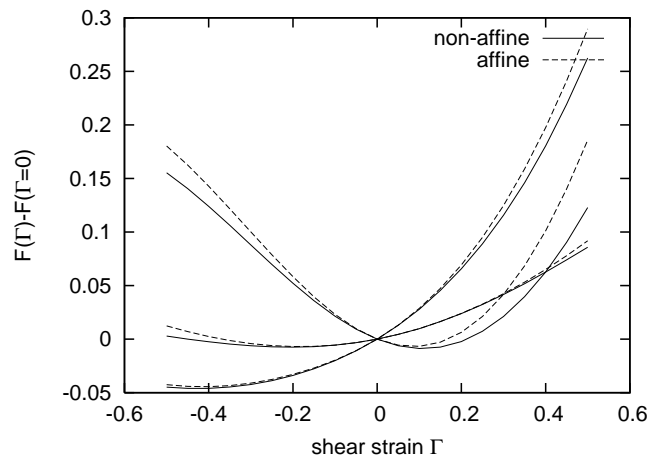


**Fig. 5.** Free energy change with shear  $\Gamma$  for three different realizations of a test polymer in a network.

value of the free energy differs strongly with the actual obstacle configuration all plots have been rescaled to the free energy value at  $\Gamma = 0$ . Obviously, for a single polymer in different specific realizations of obstacle disorder and different orientations of the plane of observation to the applied shear the resulting form of the free energy is highly variable. Furthermore, the free energy minimum is in general not at the point of zero shear. This feature however, should of course be fulfilled for the free energy function that is obtained by summing up all constituents in an macroscopic sample at equilibrium. We chose to use this requirement as a verification for an sufficient sampling over disorder. The location of the accumulated free energy minimum initially strongly oscillates with the number of samples but finally converges to  $\Gamma = 0$ . For every data point we average over a sufficient number of disorder samples until this criterion is fulfilled.

An example of the resulting averaged free energy function is shown in Fig. 6. As expected the minimum is at zero shear where the system is at equilibrium. At the application of small shear the free energy rises in a harmonic fashion which would entail a linear restoring force in an experimental measurement. Furthermore, it can be seen that the free energy obtained in the affine approximation is always above the non-affine free energy that was obtained by the minimization procedure explained above. We determine the modulus by an harmonic fit at small shear strains. At higher strains however, the free energy function is no longer faithfully described by this fit, but features a stronger slope. This signifies the onset of non-linear forces.

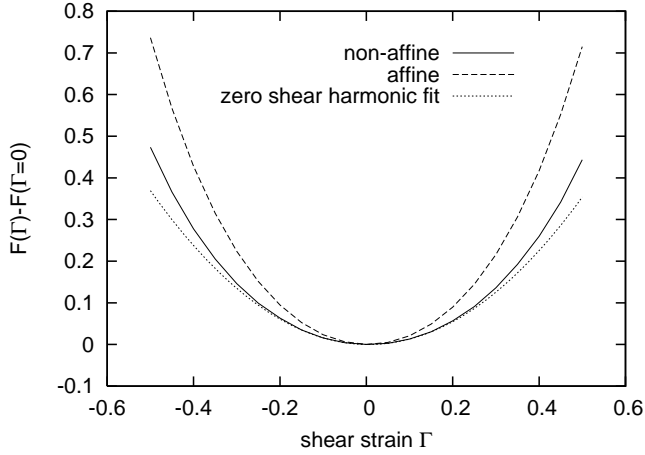


**Fig. 6.** Free energy change obtained by averaging over quenched disorder and orientation where the lower free energy curve is due to energy minimized non-affine deformations. Harmonic fits are only a valid approximation in the linear regime at small shears.

#### 4.1 Affine vs. Non-Affine

We determined the resulting plateau moduli as a function of different system parameters. Fig. 7 illustrates the scaling of the modulus with polymer concentration  $c$ . Both the

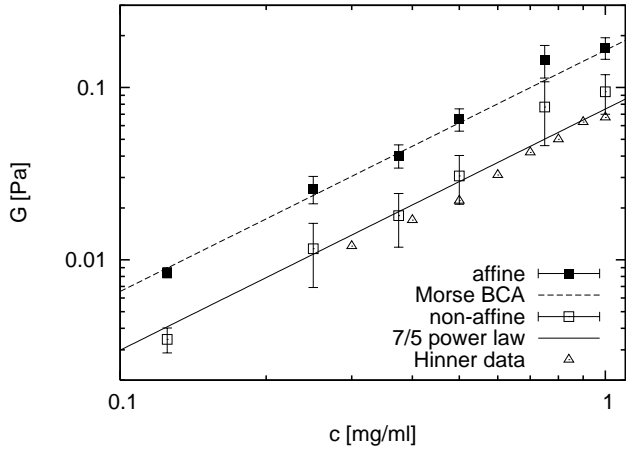


**Fig. 7.** Moduli resulting from affine and non-affine displacement of the tube contour as a function of actin concentration comply with a 7/5 power law. The affine modulus (filled squares) is in the range of the prediction by Morse [14] while the non-affine modulus (open squares) is a factor two to three lower but slightly above the experimental measurements (open triangles) by Hinner [23].

affine and the non-affine modulus show good agreement to a 7/5 power law with concentration. The non-affine modulus is considerably below the affine modulus. This confirms the initial assumption that a deformation field that assumes affine displacement on all length scales indeed overestimates the system’s response. The non-affine deforma-

tion that is obtained by permitting the engaged polymer to find its tube of minimal free energy leads to a lower modulus. Comparing the moduli from our affine calculation with the prediction for the absolute plateau modulus by Morse’s “Binary Collision Approximation” [14], shows sound consistency. In the realm of the restriction of affine displacement, our work can be seen as a numerical confirmation. However, the moduli obtained by experimental measurements [23] are considerably lower and prove that the physical reality is closer to a non-affine deformation field. Of course, the detailed nature of this field is not accessible to experiments but our data suggests that the proposed model of an affine displacement of neighbors combined with an non-affine displacement of the tube is an appropriate approximation. The non-affine moduli obtained by this approach only show slight overestimations of the experimental results and it can be argued that this is due to possible additional non-affinities in the obstacle displacement.

#### 4.2 Scaling with Persistence

Finally, we determined the scaling of the plateau modulus with persistence length  $l_p$ . The decrease of the modulus with increasing polymer stiffness is depicted in Fig. 8 and shows good agreement with a power law of  $-1/5$ . The persistence dependence represents a sensible method

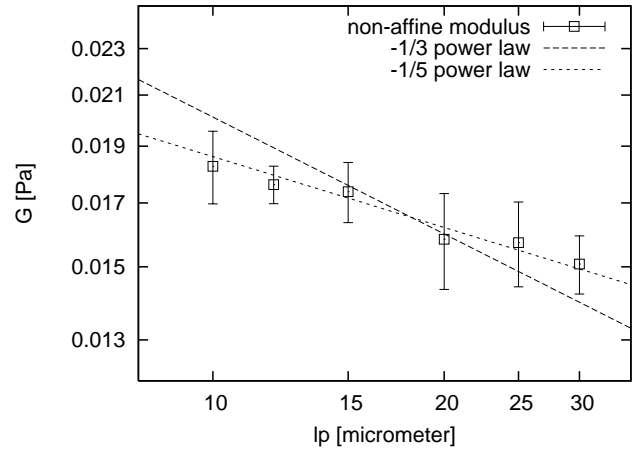


**Fig. 8.** The non-affine plateau modulus clearly shows a  $-1/5$  power law dependence on persistence length.

to discriminate between competing models of viscoelasticity. Since the value of the concentration scaling exponent  $4/3$  predicted by an effective medium approach [14] is numerically quite close to the exponent  $7/5$  predicted by most other theories, experimental accuracy does not allow for a verification. The difference of the two concepts in the persistence length scaling exponents is considerably larger:  $-1/3$  versus  $-1/5$ . Contrary to recent experiments [26] our data is clearly incompatible with an exponent of  $-1/5$ . We therefore conclude that the plateau modulus of

entangled networks of semiflexible polymers is correctly described by

$$G \propto c^{7/5} l_p^{-1/5}. \quad (14)$$

## 5 Conclusion

We have presented numerical results for the plateau modulus of entangled network of semiflexible polymers for a wide parameter range for both an affine and non-affine shear deformation field. To this end we have developed an approach that permits to approximately calculate the partition sum and the free energy of a polymer network. This was achieved by analyzing the free energy of one component of the transversal fluctuations of a test polymer in a two dimensional reference frame. Averaging over disorder and all possible reference frames results in a measure for the systems free energy. The approach allows to probe the system's free energy change and thereby mechanical response to macroscopic and microscopic deformation fields. While existing theories for the modulus of polymer networks are based on the assumption of an affine shear deformation on all length scales, we challenged this assumptions. Indeed, it was found that the free energy of the affine deformation can be reduced by allowing the tube contour of a test polymer to minimize the global energy. We observed non-affine moduli that agree well with experimental data, while existing theoretic predictions coincide with the results of our considerably higher affine moduli. Furthermore, we clearly confirm a scaling of the plateau modulus with persistence length and concentration as  $G \propto c^{7/5} l_p^{-1/5}$ . Our results prove that shear deformation of networks of entangled polymers has to be described in a non-affine picture and that affine theories systematically overestimate the mechanical response. The presented approach provides a numerical solution to evaluate complex partition sums and has a wide applicability to rheology of polymer networks. Future applications can e.g. investigation of non-linear shear.

We acknowledge support from the DFG through grant Fr 850/6-1, from the German Excellence Initiative via the NIM program and from the Elite Network of Bavaria through the NBT program.

## A Shear Deformation

We work with two coordinate systems: a three dimensional real space system and a two dimensional system in the plane of observation, where the origin of both systems is one end of the initial test polymer. The orientation of the end-to-end vector  $\mathbf{R}$  of an arbitrary test polymer in the three dimensional space is isotropically distributed. As depicted in Fig. 9 it is described by the two angles  $\theta$  and  $\phi$ . To define a plane of fluctuations we need one additional angle  $\psi$ . This plane is spanned by the vectors  $\mathbf{R}$  and  $\mathbf{S}$  with  $\mathbf{S} \perp \mathbf{R}$ . For  $\psi = 0$  the vector  $\mathbf{S}$  is obtained by applying the same transformation to an vector parallel to

the z-axis, that is needed to transform an vector parallel to the x-axis to  $\mathbf{R}$ . Other values of  $\psi$  are obtained by an rotation around the axis  $\mathbf{R}$ . Graphically it is helpful to picture the observation plane as the plane that is obtained by applying two transformations to the x-z-plane: first a rotation around the z-axis by  $\phi$  and then a rotation around the axis  $\mathbf{R}$  by  $\psi$ . If  $\mathbf{R}$  and  $\mathbf{S}$  are normalized they correspond to the x and y-axis in the plane of observation.

If we now apply a macroscopic shear deformation  $\mathcal{T}(\Gamma)$  with shear parameter  $\Gamma$  to the three dimensional system the obstacle points and the test polymer deform according to the action of the transformation  $\mathcal{T}$  on their real space coordinates. In general this signifies that they leave the plane of observation spanned by  $\mathbf{R}$  and  $\mathbf{S}$ . It is however, self-evident that also the test polymer's fluctuations are subjected to the shear and therefore also the plane of observation transforms according to  $\mathcal{T}$ . This is tantamount to a transformation of the vectors  $\mathbf{R}$  and  $\mathbf{S}$  and leaves the transformed obstacle points in the new plane of observation. We obtain the new plane coordinates in terms of the transformed unit vectors  $\mathbf{R}'$  and  $\mathbf{S}'$  that correspond again to x and y-axis. The former is obtained as  $\mathbf{R}' = \mathcal{T}(\Gamma)\mathbf{R}$  and the latter is constructed as the component of  $\mathcal{T}(\Gamma)\mathbf{S}$  that is orthogonal to  $\mathbf{R}'$ .

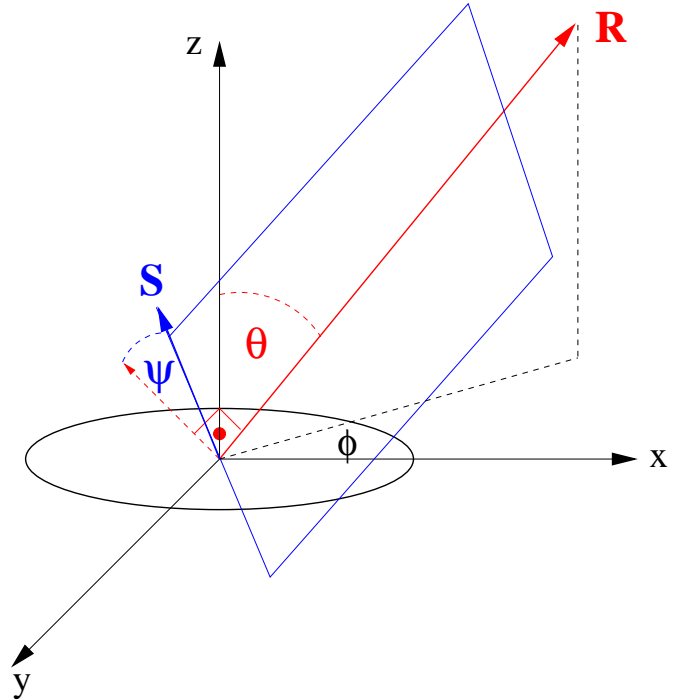


Fig. 9. Schematic illustration of the plane of observation.

## References

1. M. Doi and S. F. Edwards. *The Theory of Polymer Dynamics*. Clarendon Press, Oxford, 1986.
2. M. Rubinstein and R.H. Colby. *Polymer Physics*. Clarendon Press, Oxford, 2003.



3. N. Saito, K. Takahashi, and Y. Yunoki. *J. Phys. Soc. Jpn.*, 22:219, 1967.
4. O. Kratky and G. Porod. *Rec. Trav. Chim.*, 68:1106, 1949.
5. Jan Wilhelm and Erwin Frey. *Phys. Rev. Lett.*, 77(12):2581, 1996.
6. P. G. de Gennes. *Scaling Concepts in Polymer Physics*. Cornell University Press, Ithaca, NY, 1979.
7. F. C. MacKintosh, J. Käs, and P. A. Janmey. *Phys. Rev. Lett.*, 75:4425, 1995.
8. J.H.Shin, M.L. Gardel, L.Mahadevan, P. Matsudaira, and D.A.Weitz. *Proc. Nat. Acad. Sci.*, 101:9636, 2004.
9. Jan Wilhelm and Erwin Frey. *Phys. Rev. Lett.*, 91:108103, 2003.
10. David A. Head, Alex J. Levine, and F. C. MacKintosh. *Phys. Rev. Lett.*, 91:108102, 2003.
11. Claus Heussinger and Erwin Frey. *Phys. Rev. Lett.*, 97:105501, 2006.
12. F. Amblard, A. C. Maggs, B. Yurke, A. N. Pargellis, and S. Leibler. *Phys. Rev. Lett.*, 77:4470, 1996.
13. F. Gittes, B. Schnurr, P.D. Olmsted, F.C. MacKintosh, and C.F. Schmidt. *Phys. Rev. Lett.*, 79(17):3286, 1997.
14. D. C. Morse. *Phys. Rev. E*, 63:031502, 2001.
15. M.L. Gardel, M.T. Valentine, J.C. Crocker, A.R. Bausch, and D.A.Weitz. *Phys. Rev. Lett.*, 91(15):158302, 2003.
16. Klaus Kroy and Jens Glaser. *New J. Physics*, 9:416, 2007.
17. C. Semmrich, T. Storz, J. Glaser, R. Merkel, A. R. Bausch, and K. Kroy. *Proc. Natl. Acad. Sci. USA*, 104:20199, 2007.
18. J. Xu, Y. Tseng, and D. Wirtz. *J. Biol. Chem.*, 275(46):35886, 2000.
19. Christine Semmrich, Ryan J. Larsen, and Andreas R. Bausch. *Soft Matter*, 4:1675, 2008.
20. David C. Morse. *Macromolecules*, 31:7044, 1998.
21. H. Isambert and A. C. Maggs. *Macromolecules*, 29:1036, 1996.
22. Klaus Kroy and Erwin Frey. *Phys. Rev. Lett.*, 77(2):306, 1996.
23. B. Hinner, M. Tempel, E. Sackmann, K. Kroy, and E. Frey. *Phys. Rev. Lett.*, 81:2614, 1998.
24. W.H. Schwarz J. Xu, J.A. Kas, T.P. Stossel, P.A. Janmey, and T.D. Pollard. *Biophys. J.*, 74:2731, 1998.
25. M. L. Gardel, J. H. Shin, F. C. MacKintosh, L. Mahadevan, P. Matsudaira, and D. A. Weitz. *Science*, 304:1301, 2004.
26. M. Tassieri, R.M.L.Evans, L. Barbu-Tudoran, G.N.Khaname, J. Trinick, and T. A. Waigh. *Phys. Rev. Lett.*, 101:198301, 2008.
27. Felix Höfling, Tobias Munk, Erwin Frey, and Thomas Franosch. *J. Chem. Phys.*, 128:164517, 2008.
28. Felix Höfling, Tobias Munk, Erwin Frey, and Thomas Franosch. *Phys. Rev. E*, 77:060904, 2008.
29. A. N. Semenov. *J. Chem. Soc. Faraday. Trans.*, 82:317, 1986.
30. H. Hinsch, J. Wilhelm, and E. Frey. *E. Phys. J. E*, 24:35, 2007.
31. T. Odijk. *Macromolecules*, 16:1340, 1983.
32. T. Burkhardt. *J. Phys. A.*, 28:629, 1995.
33. Hauke Hinsch and Erwin Frey. *to be published*, 2009.
34. William H. Press, Saul A. Teukolsky, William T. Vetterling, and Brian P. Flannery, editors.
35. J.A. Nelder and R. Mead. *Comp. J.*, 7(4):308, 1965.